

# Investigations on nucleophilic layers made with a novel plasma jet technique

T. Neubert<sup>1</sup>, K. Lachmann<sup>1</sup>, M. Thomas<sup>1</sup>, V. Zeren<sup>1</sup>, J. Lips<sup>1</sup>, P. Scopece<sup>2</sup>, E. Verga Falzacappa<sup>2</sup>,  
A. Patelli<sup>3</sup>, C.-P. Klages<sup>1</sup>

<sup>1</sup>Fraunhofer Institute for Surface Engineering and Thin Films IST, Braunschweig, Germany

<sup>2</sup>Nadir S.r.l., Venezia, Italy

<sup>3</sup>Dept. of Physics and Astronomy - University of Padova, Padova, Italy

**Abstract:** In this work a novel plasma jet technique is used for the deposition of nucleophilic films based on (3-aminopropyl)trimethoxysilane at atmospheric pressure. Film deposition was varied with regard to duty cycles and working distance. Spectral ellipsometry and chemical derivatization with 4-(trifluoromethyl)benzaldehyde using ATR-FTIR spectroscopy measurements were used to characterize the films. It was found that the layer thickness and the film composition are mainly influenced by the duty cycle.

**Keywords:** plasma jet, duty cycle, pp-APTMS, derivatization

## 1. Introduction

3D-printed biodegradable polymer scaffolds for tissue regeneration are an emerging field of research [1, 2]. For optimal growing conditions of adherent cells the surface chemistry of the scaffolds can be modified by plasma treatment. Plasma-polymerized (3-aminopropyl)trimethoxysilane (pp-APTMS) for example is known to provide good cell adhesion [3]. However, conventional Dielectric Barrier Discharge (DBD) processes are hard to apply for 3-dimensional porous structures like scaffolds, especially during the printing process and for area-selective deposition as it is intended in the future. For that reason, film deposition of pp-APTMS using a plasma jet was investigated in this work. The special design of the plasma jet permits the generation of a plasma with a low energy flux to avoid thermal degradation of the 3D-printed polymers [4, 5].

## 2. Experimental

The plasma jet provided by Nadir S.r.l. consists of three coaxial tubes (Fig. 1) to separate precursor gas, process gas and shield gas from each other:

- precursor gas: 2 slm argon (purity 99.999 %) passing through APTMS (purity 96 %, abcr GmbH)
- process gas: 10 slm argon (purity 99.999 %)
- shielding and cooling gas: 20 slm N<sub>2</sub> (purity 99.999 %)

The main feature of the plasma jet is that it is powered with a high-voltage (HV) generator pulsed with 16 kHz to stabilize the plasma and a radio-frequency (RF) generator with 27 MHz to power the plasma. Deposition processes were performed on 150 μm thick polyethylene (LDPE foils from RKW SE) and niobium oxide coated soda-lime glass slides. The plasma jet was mounted on a dispensing robot "I&J 7100" from Fisnar®. For the deposition process a square area of 20 x 20 mm<sup>2</sup> was scanned with a speed of 1 mm s<sup>-1</sup> and a line width of 1 mm.

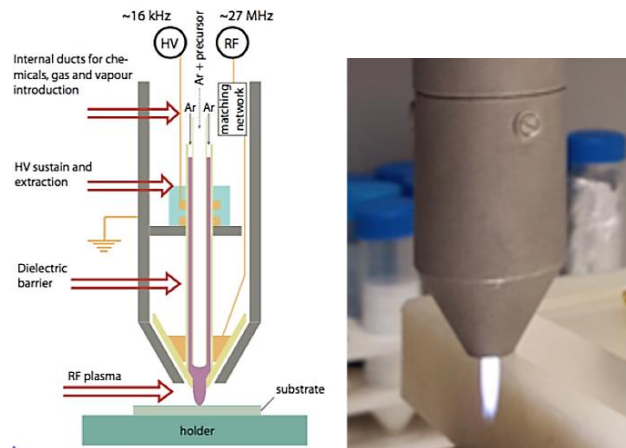


Fig. 1. Plasma jet setup from Nadir SRL

The heating power delivered to the substrate  $P_H$  of the plasma jet was determined by describing the temperature increase of a thermally isolated alumina plate (24.1 x 24.1 x 0.5 mm<sup>3</sup>), with known heat capacity  $C = 0.86 \pm 0.04$  J/K and a thermal PT100 resistor on the backside using formulae 1 and 2 [6].

$$T(t) = T_{max} - A \cdot \exp[-R \cdot t] \quad (1)$$

$$P_H = C \cdot A \cdot R \quad (2)$$

The thickness of the deposited pp-APTMS layers was measured by spectral ellipsometry on soda-lime glass substrates with a 100 nm ± 5 nm sputtered niobium oxide layer using a spectral ellipsometer "SE 850 DUV" from Sentech GmbH. The niobium oxide layer is necessary since the refractive indices of the glass substrate and the plasma polymer are very similar.

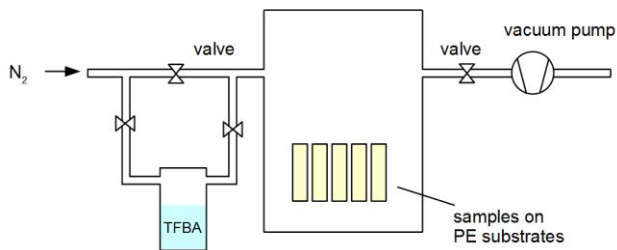


Fig. 2. Setup for the derivatization of the samples with TFBA

It is known that 4-(trifluoromethyl)benzaldehyde (TFBA) reacts with nucleophilic groups like amino or imino groups [7]. The derivatization was performed in a stainless steel reactor sketched in Fig. 2 with a diaphragm pump type “MD 4T” from Vacuubrand. For the experiments TFBA (purity 98 %) from Sigma-Aldrich and N<sub>2</sub> (purity 99.999 %) were used. Derivatization was performed within 24 h after deposition to avoid aging effects. The procedure consists of the following steps:

1. Heating to 100 °C for 1 h and evacuating the reactor to remove residues of previous processes
2. Cooling down to room temperature (1 h) + purging with 1 slm N<sub>2</sub> gas
3. Placing the samples in the reactor
4. Evacuation of the reactor for 5 min to remove adsorbates and non-reacted precursor residues
5. Opening the valve of the TFBA bottle and purging the TFBA with 100 sccm N<sub>2</sub> for 2 h to provide TFBA vapors to the samples
6. Evacuating the samples for 2 h to remove non-reacted TFBA

ATR-FTIR measurements on LDPE substrates were taken with a “Nicolet is10” FTIR spectrometer (Thermo Scientific) with a single reflection diamond ATR crystal before and after the derivatization. The density of nucleophilic groups  $\rho$  can be calculated according to reference [7] by formula 3 from the peak area  $A_{CF}$  (1335-1315 cm<sup>-1</sup>), the number of reflections on the ATR crystal ( $N = 1$ ), the ratio  $f$  of effective thickness  $d_e$  and the film thickness  $d$  of the derivatized layer and the experimentally determined integrated band intensity ( $B = 3.7 \times 10^5$  m mol<sup>-1</sup> [7]). Since the used FTIR spectrometer has no polarization filter,  $f = 4.75$  was calculated as average from the parallel and orthogonal case according to formulae 4a and 4b [8] with  $n_{ij} = n_i/n_j$ ,  $n_1 = 2.4$  for diamond,  $n_2 \approx n_3 = 1.5$  for the derivatized layer and pp-APTMS as well as PE, and an incident angle of  $\theta = 42^\circ$ .

$$\rho = \frac{A_{CF} \cdot \ln(10)}{N \cdot f \cdot B} \quad (3)$$

$$f_{\perp} = \frac{d_{e\perp}}{d} = \frac{4n_{21} \cos\theta}{1 - n_{31}^2} = 3.03 \quad (4a)$$

$$f_{\parallel} = \frac{d_{e\parallel}}{d} = \frac{4n_{21} \cos\theta [(1+n_{32}^4) \sin^2\theta - n_{31}^2]}{(1-n_{31}^2)[(1+n_{31}^2) \sin^2\theta - n_{31}^2]} = 6.47 \quad (4b)$$

### 3. Results and Discussion

In a first step the heating power of the jet was determined. As it can be seen in Fig. 3 the heating power is only about 3.5-4.5 W with a very low influence of the nozzle-to-substrate distance. The measured values for the heating power correlate well with similar measurements with other rf plasma jets, were 15 % of the total rf power input [9] and 145-160 mW [10] with a rf power input of 3.5 W [11] were reported, respectively. The maximum temperature of the alumina probe measured was between 50 and 60 °C. It is expected that such low temperatures neither lead to thermal degradation of the PE substrates nor to the polymeric material used for the scaffolds in the future.

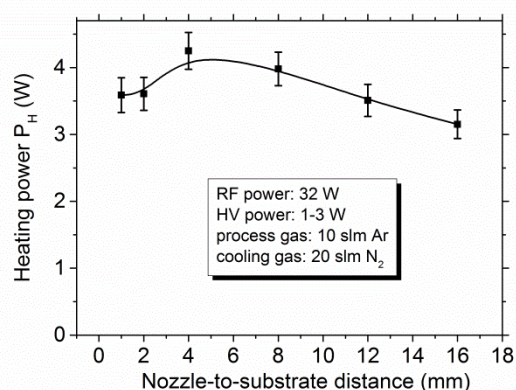


Fig. 3. Heating power of the working plasma jet to a non-conducting substrate as a function of nozzle-to-substrate distance

Synchronous pulsing of both (HV and RF) generators offers the possibility to preserve the monomer structure and thus the primary amino groups (-NH<sub>2</sub>) of the APTMS precursor. To investigate the influence of the pulsing on the layer properties the duty cycle (ratio of on-time and total period) was varied with the process parameters according to Table 1.

Table 1. Process parameters for the deposition

Scanning area	20 x 20 mm <sup>2</sup>
Scanning speed	1 mm/s
Line width	1 mm
HV power (16 kHz)	1 – 3 W
RF power (27 MHz)	15 W
On time	25 ms
Off time	0 – 500 ms
Duty cycle	100 % - 4.8 %
Working gas flow	10 + 2 slm Ar
Precursor gas flow	0.59 sccm APTMS
Shielding and cooling gas	20 slm N <sub>2</sub>
Nozzle-to-substrate distance	1 mm, 4 mm, 8 mm

It was observed that the layer thickness correlates strictly linear with duty cycle  $D$  for  $D < 50$  %. However,

for larger duty cycles ( $D > 50\%$ ) and short nozzle-to-substrate distances the yield is reduced (Fig. 4). This behaviour could be explained by competing etching processes for short distances. There is only a weak influence of nozzle-to-substrate distance on the thickness for short distances.

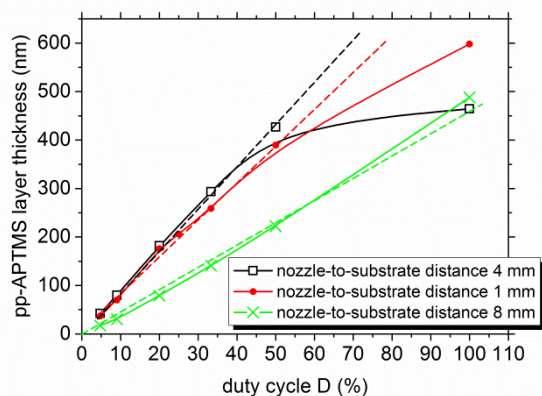


Fig. 4. Thickness of the deposited pp-APTMS layers as a function of the duty cycle  $D$

As expected we found a significantly increased density of nucleophilic groups for low duty cycles (Fig. 5). The highest density of nucleophilic groups was found for low duty cycles (9%) and larger distances (8 mm) with 2.3 groups per  $\text{nm}^2$ . As comparison for evaporated APTMS layers (polymerized with  $\text{H}_2\text{O}$  from the air humidity) we found values in the range of  $6.8 \pm 1.7$  groups per  $\text{nm}^2$ . This seems to be the maximum value of primary amino groups achievable with APTMS. It is already known from former experiments using a conventional DBD setup and glycidylmethacrylate (GMA) as precursor that low duty cycles lead to a retention of the monomer structure [12].

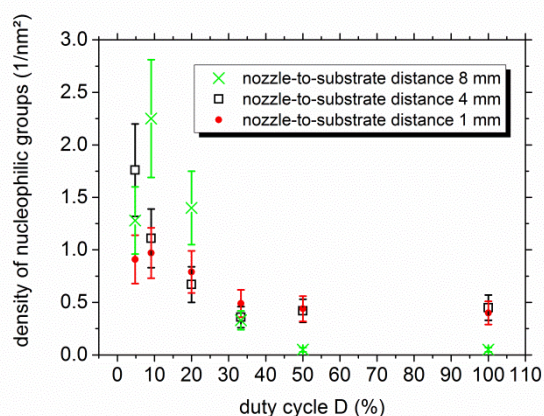


Fig. 5. Density of nucleophilic groups of pp-APTMS layers as a function of duty cycle  $D$

Although in this investigation a monomer with a C-C double bond was used, similar behaviour is confirmed for pp-APTMS in the current experiments. Fig. 6 shows

that pp-APTMS layers made with low duty cycles have a higher content of Si-O-CH<sub>3</sub> vibrations at 1190 and 1100  $\text{cm}^{-1}$  than layers made with a high duty cycle, which have more Si-O-Si vibrations at 1090-1010  $\text{cm}^{-1}$ , according to [13].

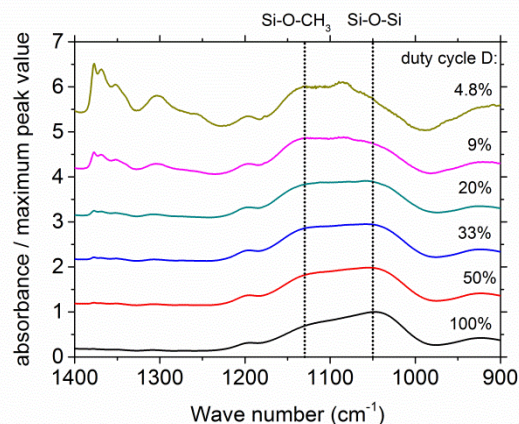


Fig. 6. ATR-FTIR spectra of pp-APTMS (nozzle-to-substrate distance 8 mm) layers for various duty cycles  $D$

#### 4. Conclusion and Outlook

In this work we have demonstrated the possibility to deposit chemically reactive plasma-polymerized APTMS thin films using a plasma jet. By varying the deposition conditions it is possible to modify the density of functional groups and the film composition, as well as the deposition rate. Future experiments will deal with the chemical stability and long-term stability of such layers against incubation in different solvents and storage in different atmospheres, e.g.. Moreover, 3-dimensional substrates will be modified.

#### 5. Acknowledgements

Results of this work were funded by the European Union's Horizon 2020 research and innovation programme under grant agreement No 685825.

#### 6. References

- [1] S. Stratton, N. B. Shelke, K. Hoshino, S. Rudraiah, S. G. Kumbar, *Bioact. Mater.* 1, 93-108 (2016).
- [2] L. Moroni, J.R. de Wijn, C.A. van Blitterswijk, *Biomaterials* 27, 974-985 (2006).
- [3] A. M. C. Barradas, K. Lachmann, G. Hlawacek, C. Frielink, R. Truckenmoller, O. C. Boerman, R. van Gestel, H. Garritsen, M. Thomas, L. Moroni, C. van Blitterswijk, J. de Boer, *Acta Biomater.*, 8, 2969-2977 (2012).
- [4] A. Patelli, et al., 4th International Conference on Cultural Heritage, EuroMed 2012; Limassol; Cyprus; 29 October – 3 November 2012. Volume 7616 LNCS, 793-800, (2012).
- [5] F. Mussano, T. Genova, E. Verga Falzacappa, P. Scopece, L. Munaron, P. Rivolo, P. Mandracci, A. Benedetti, S. Carossa, A. Patelli, *Appl. Surf. Sci.*, in press, <http://dx.doi.org/doi:10.1016/j.apsusc.2017.02.035>.

- [6] S. Bornholdt, T. Peter, T. Strunskus, V. Zaporozhchenko, F. Faupel, H. Kersten, *Surf. Coat. Tech.* 205, 388-392 (2011).
- [7] C.-P. Klages, A. Hinze, Z. Khosravi, *Plasma Process. Polym.* 10, 948-958 (2013).
- [8] N. J. Harrick, *Appl. Optics.* 10, 19-23 (1971).
- [9] J. Janca, M. Klima, P. Slavicek, L. Zajickova, *Surf. Coat. Tech.* 116–119, 547–551 (1999).
- [10] M. S. Mann, R. Tiede, K. Gavenis, G. Daeschlein, R. Bussiahn, K.-D. Weltmann, S. Emmert, T. von Woedtke, R. Ahmed, *Clinical Plasma Medicine* 4 35–45 (2016).
- [11] S. Bekeschus, A. Schmidt, K.-D. Weltmann, T. von Woedtke, *Clinical Plasma Medicine* 4, 19–28 (2016).
- [12] C.-P. Klages, K. Höpfner, N. Kläke, R. Thyen, *Plasma Polym.* 5, 79-89 (2000).
- [13] G. Socrates, *Infrared and Raman Characteristic Group Frequencies*, Third Edition, John Wiley & Sons, LTD, 241-246 (2001)